

A laboratory study of breaking waves*

OCEANOLOGIA, 46 (3), 2004.
pp. 365–382.

© 2004, by Institute of
Oceanology PAS.

KEYWORDS

Breaking waves
Tank experiment

JAROSŁAW TĘGOWSKI

Institute of Oceanology,
Polish Academy of Sciences,
Powstańców Warszawy 55, PL–81–712 Sopot, Poland;
e-mail: tegowski@iopan.gda.pl

Manuscript received 23 March 2004, reviewed 2 August 2004, accepted 5 August 2004.

Abstract

This paper deals with some aspects of the wave-breaking phenomenon. The objectives were to study wave-breaking criteria, and the probability of whitecap coverage under fully controlled wave conditions. An additional task was to investigate the characteristic spectral features of the noise produced by breaking waves and the acoustic energy generated during wave breaking events. A controlled experiment was carried out in the Ocean Basin Laboratory at MARINTEK, Trondheim (Norway). Waves were generated by a computer-controlled multi-flap wave maker, which reproduced a realistic pattern of the sea surface for the prescribed spectra. Using wave staff recordings and photographic techniques, correlations between the breaking parameters and the radiated acoustic emissions were established.

1. Introduction

The breaking of ocean waves plays an important role in all aspects of air-sea interaction processes such as momentum, mass and heat transfer (Monahan 1969, 1971, Blanchard 1971, Massel 2001a). Breaking waves are responsible for whitecap formation on the sea surface and the creation

* The experiment was funded by European Commission under the ‘Improving Human Potential Access Infrastructures’ Programme number HPRI-CT-1999-00060.

of air bubbles in the top ocean layer. Whitecaps are the principal source of marine aerosol fluxes moving from the sea to the atmosphere. Bubble clouds produced by breaking waves influence ocean reflectance and in-water light field characteristics both within the surface layer and leaving it (Stramski & Tegowski 2001). Additionally, oscillations of gas bubbles generated by breaking waves are the main source of wind-generated noise in the ocean (Ding & Farmer 1993, Kolaini & Crum 1994, Kolaini 1998, Deane & Stokes 2002).

The process of wave breaking is responsible for the dissipation of surface wave energy into the ocean. The measurement of this phenomenon requires the determination of kinematic and dynamic parameters of the breaking events, which are difficult to estimate under real sea conditions. In the present work, the frequency of breaking events, the fraction of sea surface covered by whitecaps, and the amount of dissipated energy produced by wave breaking were measured in a controlled experiment. A further aim of the experiment was to estimate the acoustic energy generated by breaking waves and the relation of this energy to the dissipation rate of breaking events. Bubbles plunging into the water column during wave breaking oscillate and are the main source of ambient noise in the ocean. For individual breakers, the noise spectral parameters of the acoustic emissions were worked out. In previous controlled experiments (Melville 1993, Kolaini & Crum 1994, Kolaini 1998), measurements of noise generated by breaking waves were performed for regular wave trains or groups of waves. The unique aspect of the present controlled experiment was the measurement of breaking parameters for realistic sea surface patterns.

2. Tank experiment description

The controlled experiment was carried out in a freshwater tank in the Ocean Basin Laboratory at MARINTEK, Trondheim (Norway), during March 2001. The experimental philosophy and methodology was presented in detail by Massel et al. (2001).

The tank was 80 m by 50 m in size and its movable bottom during the measurements was fixed at a depth of 2.5 m. Random wave spectra were generated by a multi-flap wave maker consisting of 144 individually controlled flaps located alongside the 80-m-long wall of the tank. This wave generation system was able to produce waves with a maximum height of 0.4 m. The other, a directional double-flap wave maker, was capable of generating regular waves of 0.9 m maximum height. Wave spectra were formed by using the JONSWAP spectrum (Hasselmann et al. 1973) and the directional

spreading function defined as $D(\theta) = A \cos^n(\theta)$ (θ is the wave direction, and $n = 0, 2, 10, 20, 40$). The wave height H_s varied from 0.08 to 0.60 m, the wave period T_p from 1.0 s to 2.0 s.

The water elevation was measured by 12 wave staffs positioned 3.5 m apart in front of the multi-flap wave maker. The wave staff sampling frequency was 80 Hz. Fig. 1 shows the experimental set-up.

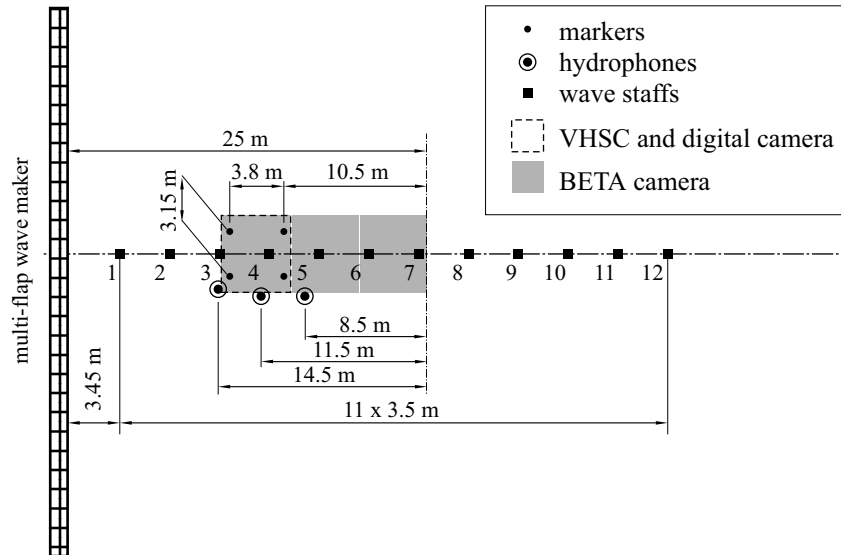


Fig. 1. Experimental set-up

The whitecap coverage and appearance of breaking events were measured by a photographic technique. The irregular water surfaces were filmed by four video cameras located 5 m above the still water level. Special image processing determined the whitecap area, as well as the length of the crest of the breaking wave, which was required to calculate the breaking wave dissipation energy. Additionally, the video records of the breaking events were used for testing the breaking criterion algorithm. The noise of breaking waves was recorded by 4 hydrophones (Bruel & Kjaer 8103) – three deployed 0.5 m below the mean water level and one 1 m deeper. Acoustic signals from the hydrophones were amplified, transmitted to an analogue-digital converter (12 bit, sampling frequency – 25 kHz or 50 kHz) and recorded in a storage device. The operator, who was in the measurement room situated above the water surface, commenced acoustic data recording for each sequence. The starting moment of the acoustic registration was recorded simultaneously with the surface elevation data and synchronized in time with the video recordings. Data were collected for 23 minutes in each of thirty tests.

3. Measurement of the wave-breaking criterion

The criterion for the breaking of regular waves in deep water has been investigated from various positions (Ochi & Tsai 1983, Weissman et al. 1984, Srokosz 1986, Xu et al. 1986, Massel 1996a, b, 1998). The most commonly known breaking criterion is given by

$$H \geq 0.142L_*, \quad (1)$$

where H – wave height, $L_* = 1.2 g/(2\pi f_w^2)$ – Stokes limiting wave length, f_w – wave frequency, g – gravitational acceleration.

In this study we tested a set of methods for detecting wave breaking, and the results obtained with the breaking criteria algorithms were compared with the video recordings. The following methods were tested:

- slope parameter ak – the threshold value of the product of the amplitude a and wave number k – (Longuet-Higgins (1975) showed that steady, periodic waves break when $ak \geq 0.443$);
- band-pass and high-pass filtering of wave elevation recordings – the measure of energy of the high frequency part of the wave spectra (Weissman et al. 1984);
- spectral parameters – especially the fourth spectral moment, which is sensitive to breaking energy dissipation (Massel 1996a);
- the fractal dimension of wave records computed in a sliding window;
- wavelet analysis – computation of the wavelet energy of wave trains (Massel 2001b, Massel et al. 2001);
- the threshold value of the first derivative of the wave elevation function $y(t)$ (Longuet-Higgins & Smith 1983).

The development of this last method yielded the best results.

Assuming that $y(t)$ is a time series of water-surface displacements measured by the wave staff (see Fig. 2a), the local slope of the interface $s(t)$ can be expressed by the temporal rate of variation $R(t)$ (Longuet-Higgins & Smith 1983) as

$$s(t) = \frac{dy}{dx} = \frac{dy}{d(C dt)} = \frac{1}{C} \frac{dy}{dt} = \frac{R(t)}{C}, \quad (2)$$

where

$$R(t) = \frac{dy(t)}{dt}, \quad C - \text{phase speed}. \quad (3)$$

From eqs. (2) and (3) we can obtain:

$$\frac{d^2y(t)}{dt^2} = C \frac{ds(t)}{dt}. \quad (4)$$

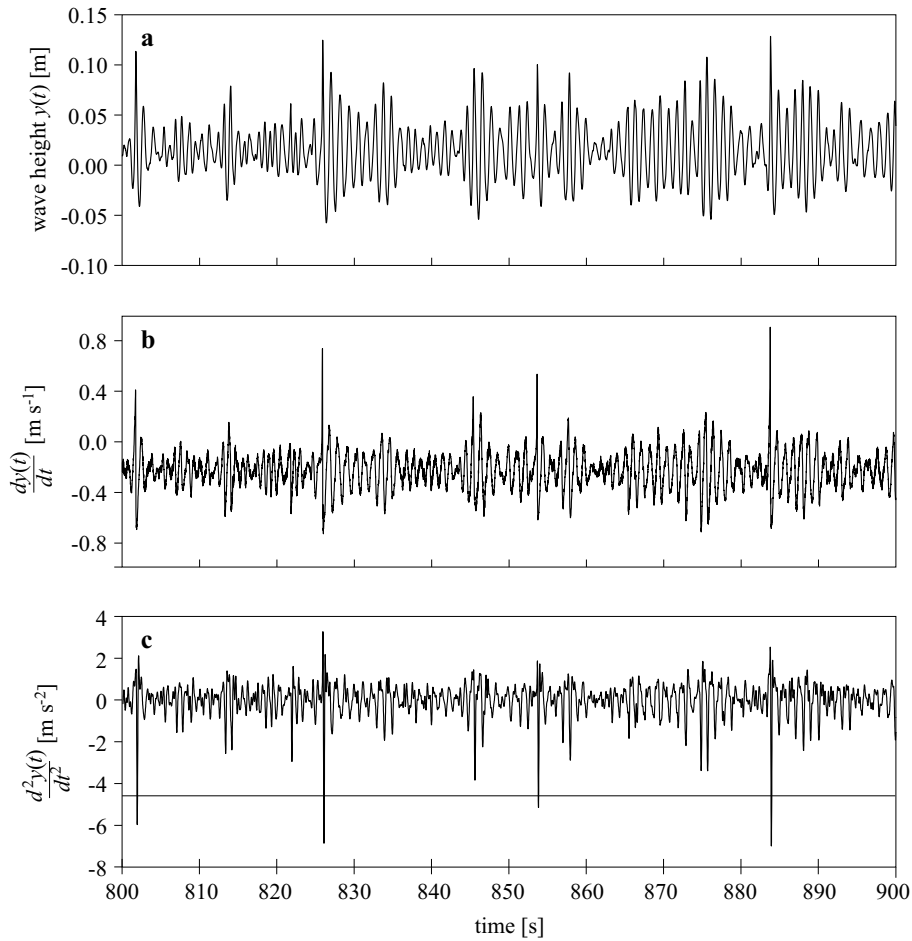


Fig. 2. (a) An example of a 100-second low-pass filtered wave train $y(t)$, (b) the first derivative of $y(t)$, (c) the second derivative of $y(t)$

The second derivative of the time series of water-surface displacements is the product of the rate of temporal variation of the surface local slope and C , the phase velocity of waves. We are forced, as it were, to use the phase velocity C , owing to the lack of information on the spatial variability of profile $\frac{dy(t)}{dx}$ if we observe wave surface changes at one point only. This is a rough assumption, which, for regular waves, holds only approximately. In the case of irregular waves we are dealing with a whole spectrum of dispersion waves, in which the individual harmonics move with different phase velocities. Note that $\frac{d^2y(t)}{dt^2}$ is a measure of the Euler acceleration of the elementary volumes of a liquid lying on the wave surface. At the instant a wave breaks, a sharp increase in the value of $R(t)$ is detected (Longuet-Higgins & Smith 1983). Longuet-Higgins & Fox (1977) demonstrated that

the maximum value of the local slope parameter $s(t)$ for regular, gravity waves is $s_{\max} = 0.586$. Longuet-Higgins & Smith (1983) used the parameter $R(t)$ to discriminate breaking waves appearing in the wave train. This method was tested in the present experiment by comparing the results of the discrimination algorithm with the video recordings. However, much better results were obtained for the algorithm by utilizing the second derivative of a time series of water-surface displacements, which is very sensitive to the rate of surface local slope variation and can be a good tool for detecting breaking events. The breaking criterion based on Stokes' theory demonstrates that deep-water waves break when the dimensionless Lagrange acceleration a_L is less than $-0.388 \times g$. The results of the experiments (Massel 1996a) show that $a_L(t) < -\alpha g$, where $\alpha \sim (0.2-0.5)$. An example of a 100-second low-pass filtered wave train $y(t)$ and the first and second derivatives of $y(t)$ are shown in Figs 2a, b, and c.

For each point in the time series, the detector function was tested to see if it was above the threshold. If the value of $\frac{d^2 y(t)}{dt^2}$ was lower than the threshold value (the horizontal line in Fig. 2c), we could expect breaking events. The threshold level was determined experimentally by comparing the results obtained from the discrimination algorithm with video observations. Thresholds were estimated for each wave experiment. For this method, overall consistency with the video observations was obtained.

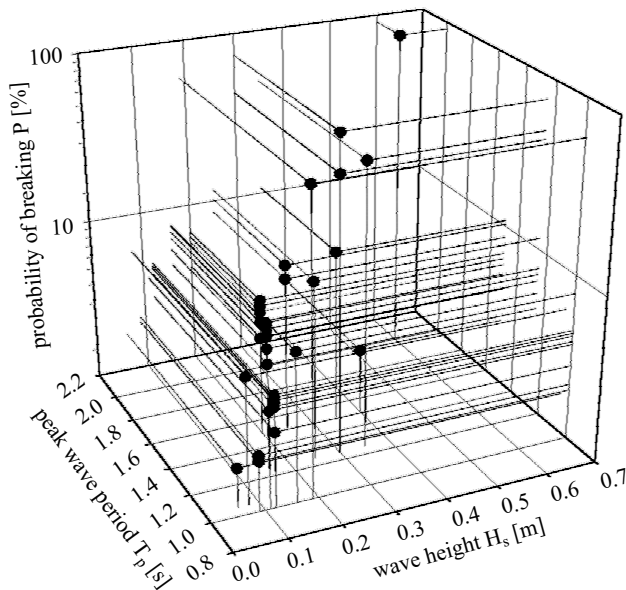


Fig. 3. The probability of breaking P [%] versus the significant wave height H_s and peak wave period T_p

The probability of breaking events is defined as $P = n_{bw}/N$, where n_{bw} is the number of breaking waves and N is the total number of waves. The result of the second derivative threshold-breaking criterion is shown in Fig. 3. This shows the probability of breaking events versus significant wave height H_s and wave period T_p . In most of the experiments, this probability did not exceed 10%. But as far as the highest and longest waves are concerned, the probability of breaking was found to exceed 40%. For comparison, the result obtained by Longuet-Higgins & Smith (1983) in the open sea at a wind speed of about 6 m s^{-1} was $P = 1.3\%$. Under similar wind conditions but with a fetch of 8 km Weissman et al. (1984) obtained $P = 8.6\%$. Thorpe & Humphries (1980) found P in the range of 2.6–6.5% for similar wind speeds. In Holthusen's (1985) measurements, P was as high as 31% for wind speeds of 12 m s^{-1} .

4. Estimation of the water fraction covered by whitecaps

In recent decades, the dependence of whitecap coverage on various environmental factors has been the object of intensive study. The relationship between wind speed and whitecap coverage area was investigated by Monahan (1969, 1971), Blanchard (1971), Toba & Chaen (1973), Ross & Cardone (1974), Monahan & O'Muircheartaigh (1980), Massel (2001a), Stramska & Petelski (2003). The dependence of wind friction velocity and wind stress was studied by Wu (1979, 1988), Monahan (1993), Kraan et al. (1995), Massel (2001a), Stramska & Petelski (2003). The correlation between energy dissipation rates of wind waves and whitecap coverage was examined by Cardone (1969), Hanson & Phillips (1999), and Massel (2001a). The large dispersion of results demonstrates the complexity between various parameters and whitecap coverage.

We investigated the dependence of whitecap coverage on significant height H_s , period T_p and different directivity spectra of the wave field without the effect of wind. Such information can be obtained using image processing methods applied to video records. The 'saturation' component of the film frame provides an estimate of the whitecap area in the most effective way. In the beginning, video recordings were converted from RGB to HSV (Hue-Saturation-Value) format. Whitecaps were observed as a separate region in the picture after thresholding and eliminating individual pixels (Massel et al. 2001). The area of whitecaps is proportional to the number of black pixels in the converted picture. This method can be applied to all frames of the video stream (25 frames per second) and produces the average whitecap area in the measured time period. The result of image processing is demonstrated in Fig. 4, which shows the dependence of whitecap coverage

on the wave parameters H_s and T_p . This result was obtained using an averaging procedure, where each point in Fig. 4 shows the average result obtained for 15 000 frames – 10 minutes of the recording stream. The whitecap area is no greater than 0.1%; only for waves of the highest energy does the whitecap area exceed 1%. Similar results were obtained for the field measurements conducted by Monahan (1969) and Monahan & Zietlow (1969).

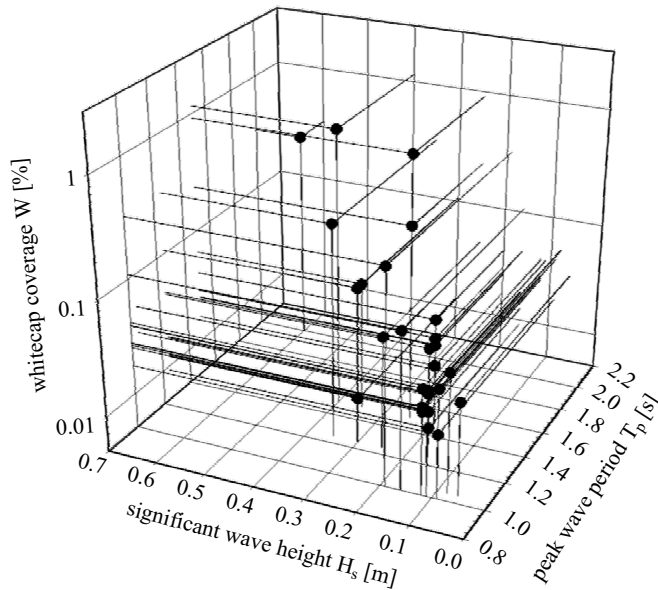


Fig. 4. Mean fraction of tank surface covered by whitecaps W [%] versus significant wave height H_s and peak wave period T_p . Averaging time – 10 minutes

It is important to note that the present experiment was performed in a tank filled by fresh water. Monahan & Zietlow (1969) tested the differences between whitecap coverage in fresh and salt water and found that for the same breaking waves the whitecap area is larger for salt than for fresh water. In salt water, large numbers of small air bubbles are created during the collapse of a breaking wave. The mechanisms of bubble surface stabilization in salt water involve contamination by surfactant additives and the absence of the coalescence retardation effect (Kolaini 1998). These mechanisms are responsible for the larger areas and the longer lifetime of salt-water whitecaps than those formed in fresh water.

5. Noise generated by breaking waves

The acoustic measurements of breaking waves were focused on two problems: the description, using spectral parameters, of consecutive phases

of noise generated by breaking events, and the estimation of the mean radiated acoustic energy generated by breaking waves versus the rate of energy dissipation in a breaking wave. Noise generated by breaking events was recorded by hydrophones placed below water surface. An example of a breaking event recorded by a line of wave staffs is shown in Fig. 5.

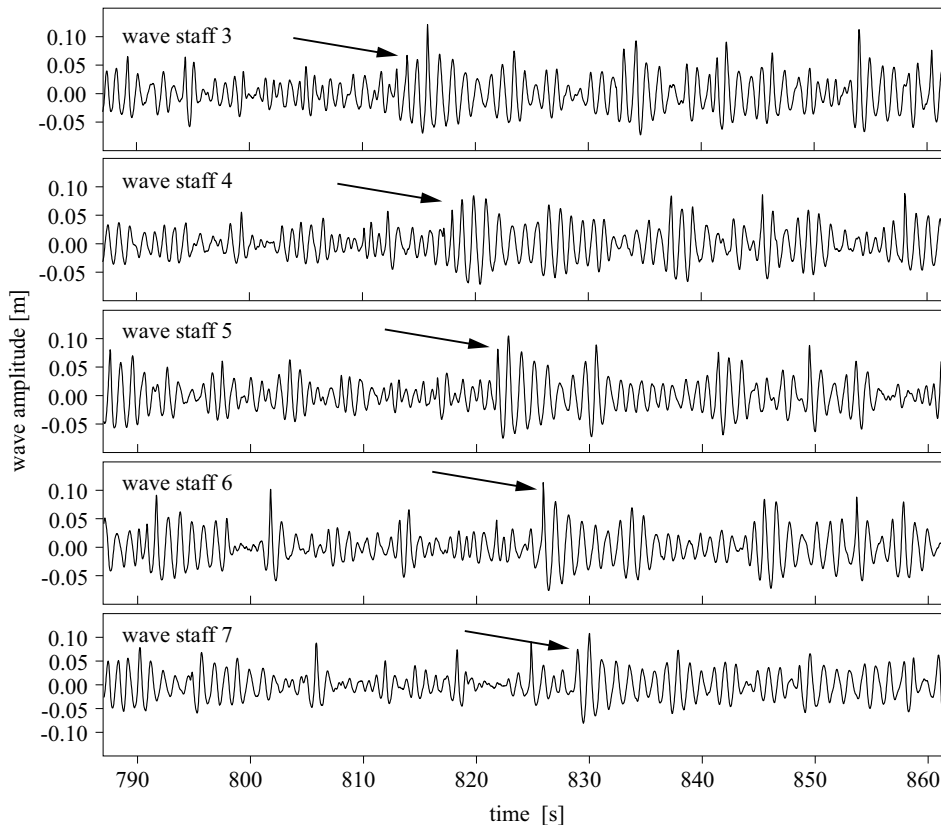


Fig. 5. Surface wave variation recorded by 5 consecutive wave staffs. The arrows indicate the time evolution of the breaking event

The arrows in the consecutive drawings in Fig. 5 indicate the time evolution of the breaking event. The start of breaking is visible at wave staff number 4 and the end in the vicinity of wave staff 6. The breaking event was verified by video recordings analyses. A hydrophone placed between staffs 4 and 5 (see Fig. 1) recorded the noise generated by the breaking event. A 1.1-second long acoustic signature of a plunging breaker was extracted from a 10-second sound record (Fig. 6).

The acoustic emission consists of several phases recorded on the spectrogram (Fig. 7). There is an increase in noise caused by the resonance

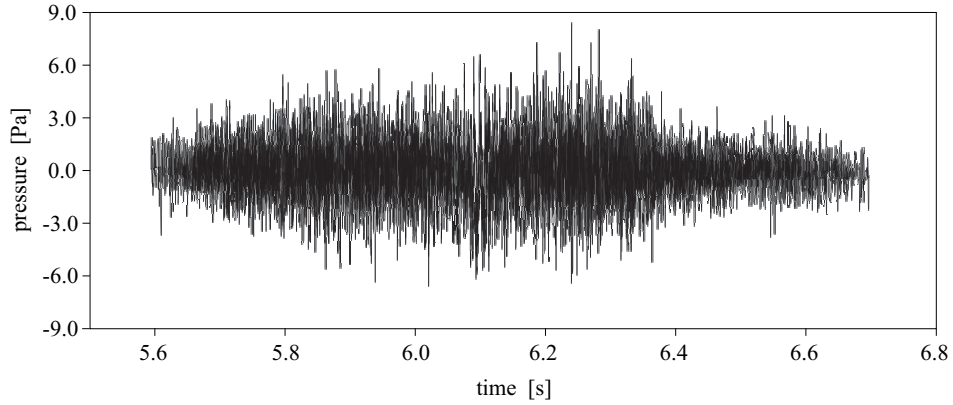


Fig. 6. Pressure-time trace of a plunging breaker

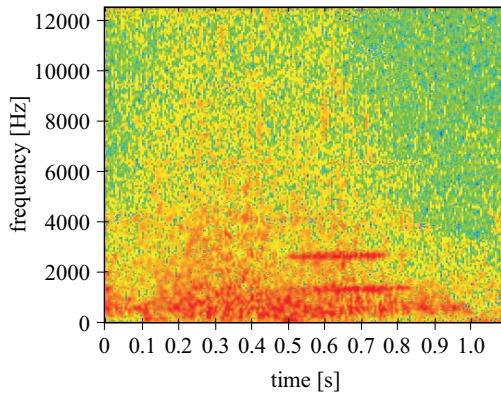


Fig. 7. Spectrogram of an acoustic signature of a plunging breaker (duration 1.1 s)

oscillations of gas bubbles at the wave crest. The wave breaks and bubbles start vibrating during the fragmentation of the air cavity formed by the plunging jet. Small bubbles are created by the division of large ones, and we can observe the group oscillations of small bubbles with low frequencies (Oguz 1994, Orris & Nicholas 2000, Deane & Stokes 2002). We can assume that a group oscillating bubble cloud is represented by an effective spherical cloud of radius R_c . The void fraction β of this structure is given by Oguz (1994):

$$\beta = \frac{4\pi\bar{n}}{3} \int_{a_{\min}}^{a_{\max}} a^3 f(a) da, \quad (5)$$

where \bar{n} is the number of bubbles per unit volume, a is the bubble radius, a_{\min} and a_{\max} are the radii of the smallest and largest bubbles, and $f_n(a)$ is

the bubble size distribution. The bubble cloud oscillates with a set of normal modes. The lowest oscillation frequency is given by Carey et al. (1993) as

$$f \approx \frac{1}{2R_c} \sqrt{\frac{P_0}{\rho\beta}}, \tag{6}$$

where ρ is the liquid density and P_0 is the ambient pressure.

The two horizontal line structures visible between 0.5 and 0.85 s are caused by the noise generated by the paddles producing the surface waves. The detailed analysis of spectrogram was carried out by dividing the acoustic signature into 14 sections of 1.1 s each and computing the spectra of each 80 ms interval of the noise signal (Fig. 8). For the first few spectra, we see an increase in the low frequencies as the result of large-bubble oscillations. The low frequency increase seen in the last two figures is the consequence of the collective oscillations of the bubble cloud. The other frequencies in the spectra are due to resonant oscillations of bubbles. The decreasing rate of spectra is from 5.5 to 6 dB per octave.

The frequency structure of the noise generated by breaking waves can be described by its spectral characteristics.

The acoustic behaviour of breaking events may be related to the spectral moments of each 80 ms interval of the noise signal:

$$m_r = \int_0^\infty \omega^r S(\omega) d\omega, \tag{7}$$

where $S(\omega)$ is the power density function of the breaking-wave event noise.

The spectral parameters are the combination of spectral moments and defined as (Massel 1996a)

$$\varpi = \frac{m_1}{m_0}, \tag{8}$$

$$\nu^2 = \frac{m_0 m_2}{m_1^2} - 1, \tag{9}$$

$$\gamma = \frac{\tilde{m}_3}{\tilde{m}_2^{3/2}}, \tag{10}$$

where ϖ – mean frequency, ν^2 – spectral width and γ – spectral skewness.

The spectral width is the measure of spectrum concentration around the mean frequency. The spectrum is extremely narrow when $\nu^2 \rightarrow 0$ but is wide when the spectral width increases. Spectral skewness γ is the measure of the spectrum symmetry and was computed for central spectral moments \tilde{m}_r .

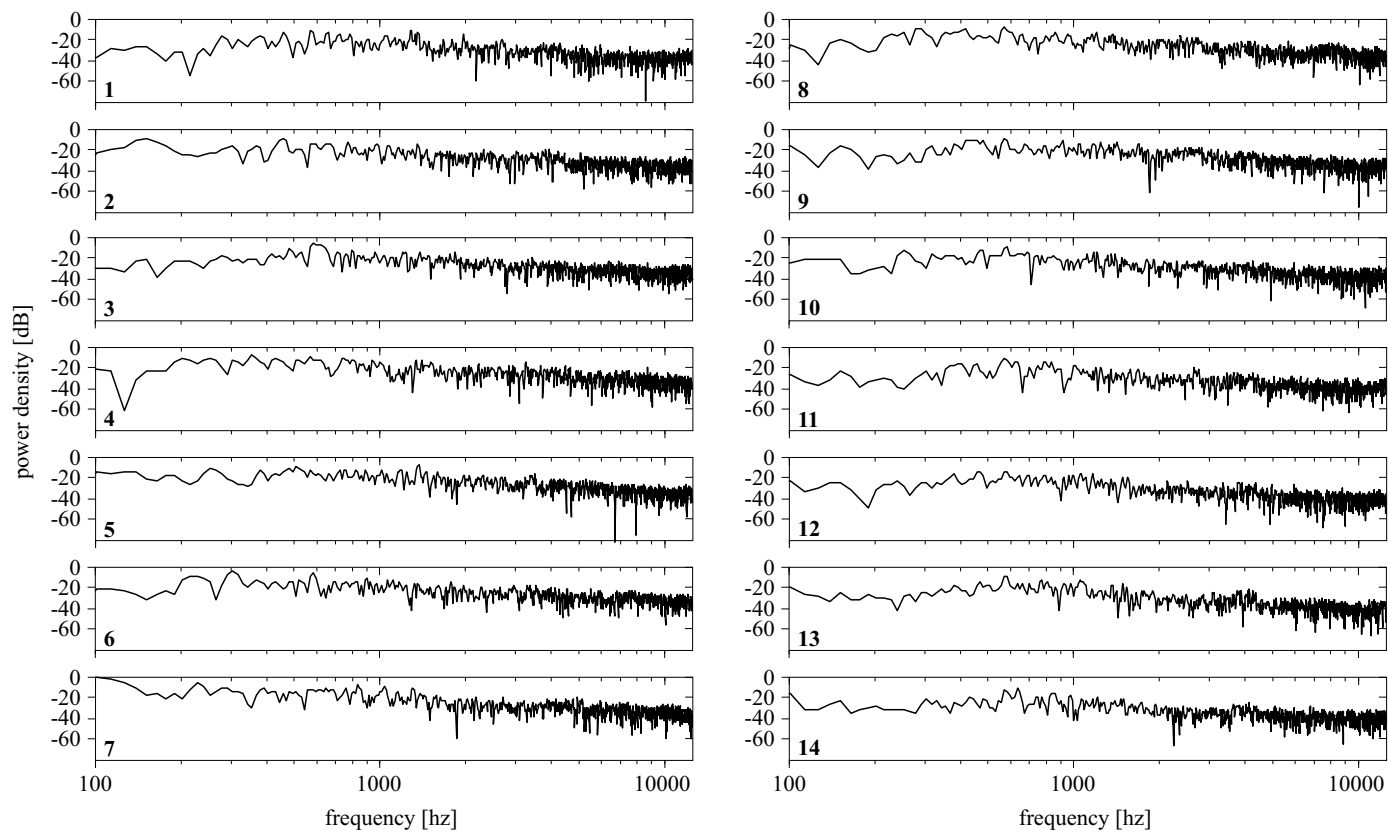


Fig. 8. Power spectra of an acoustic signature of 1.1 s duration of a plunging breaker for 80 ms intervals

Figs 9a and 9b show the results of computing the spectral width and spectral skewness of noise generated by the breaking wave event shown in Fig. 6.

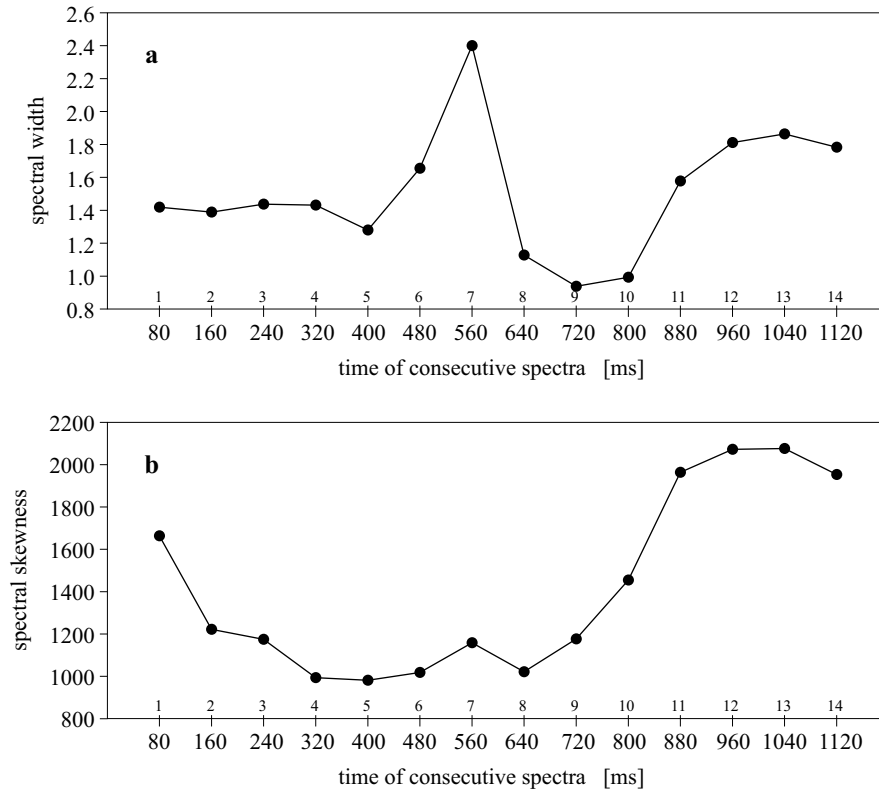


Fig. 9. (a) The spectral width and (b) the spectral skewness of the 14 consecutive spectra of plunging breaker noise shown in Fig. 8. The time interval between the spectra is 80 ms

Each dot in Fig. 9 represents the value of the spectral parameters for 80 ms intervals of noise signal. In the initial phase of the breaking event from point 1 to 4, the decrease in spectral skewness is caused by oscillating bubbles created at the wave front. Values of spectral skewness for points 5 to 7 are caused by oscillations of large bubbles created after air cavity decomposition (Dean & Stokes 2002). The increase in spectral skewness for the final points is the result of the collective oscillations of the bubble cloud.

In the top figure (9a) from point 5 to 7 there is a dramatic increase in spectral width and the spectral energy concentrates around the mean frequency. This is the result of oscillations of large bubbles of low frequencies.

The effect of the collective oscillations of the bubble cloud is visible in the few final intervals. The bottom figure 9b shows the changes in spectral skewness.

6. Energy generated by breaking waves

The ratio of the acoustic energy generated during breaking events to the energy dissipated by individual breaking waves is crucial information required for the prediction of sea state or whitecap coverage by measurement of the ambient noise level.

Pulsations of gas bubbles created by breaking waves cause the radiation of acoustic energy. We can assume a point source model and its image as a reflection from the water surface, which form an acoustic dipole. The intensity of radiated noise averaged by the time of the breaking event τ_c is (Kolaini & Crum 1994):

$$I(r, \theta) = \frac{1}{\rho_w c_w} \left[\frac{1}{\tau_{ac}} \int_0^{\tau_{ac}} P_{ac}^2 dt \right] \cos^2 \theta, \quad (11)$$

where P_{ac} is the acoustic pressure radiated by breaking event, r – the distance between the acoustic source and the receiver, θ – the angle determined by distance r , ρ_w – water density, c_w – sound speed in water.

Assuming the dipole model of the source emitting the noise of the breaking wave (Ding & Farmer 1994), the total energy is obtained by integrating the radiated intensity over a hemisphere of radius R_0 .

$$\Pi = \frac{2\pi R_0^2}{\rho_w c_w} \left[\int_0^{\tau_{ac}} P_{ac}^2 dt \right], \quad (12)$$

where R_0 is the radius centred at the point where the dipole intersects the pressure release surface.

The breaking wave energy dissipation was measured using Melville's (1993) results for the rate of energy dissipation per unit length along the wave crest ε_l :

$$\varepsilon_l \approx (3.2 \times 10^{-3}, 1.6 \times 10^{-2}) \frac{\rho_w C^5}{g}, \quad (13)$$

where C is the phase velocity of breaking waves and g is the gravitational acceleration.

The rate of energy dissipation in a breaking wave E_l is described by the following expression:

$$E_l = \varepsilon_l L_c, \quad (14)$$

where L_c is the crest length.

The mean value of numerical factor ε_l was used ($\varepsilon_l = 9.6 \times 10^{-3}$) to calculate the rate of energy dissipation per unit length along the wave crest. A similar method of computation was also used by Ding & Farmer (1993). The individual crest lengths were measured from frozen frames of video recordings with markers visible in the videos. We chose 27 out of 110 recorded acoustic signatures of breaking events because of the difficulty in estimating the length of the breaking crests. The ratio of the acoustic energy generated during breaking events to the energy dissipated by individual breaking waves is presented in Fig. 10.

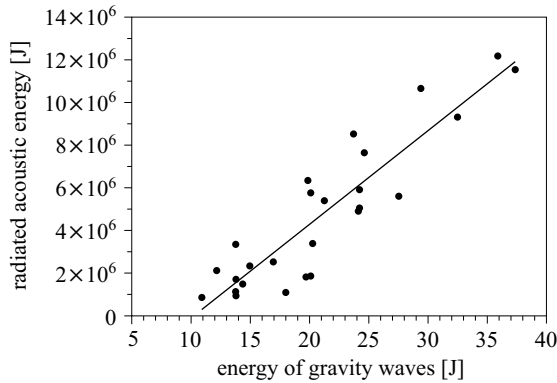


Fig. 10. Mean radiated acoustic energy generated by breaking waves versus energy dissipation in breaking waves

In these experiments, the ratio of acoustic energy to the energy dissipated in breaking waves varied from 1.0×10^{-7} to 4.1×10^{-7} , while Ding & Farmer (1994) obtained the ratio as 0.6×10^{-8} to 4.0×10^{-8} in the Pacific, 600 Nm WNW of San Diego, in an environmental experiment. In their Seneca Lake experiment, Carey et al. (1993) obtained from 0.3×10^{-8} to 2.3×10^{-8} . Higher values of this ratio were obtained in tank experiments by Kolaini & Crum (1994); they varied from 0.8×10^{-7} to 1.09×10^{-6} . This dispersion is caused by the different environmental conditions in experiments performed in the open ocean, lakes and tanks.

7. Conclusions

An experiment was performed under controlled conditions to measure the whitecap coverage, probability of breaking events and acoustic radiation generated by breaking waves. For wave parameters of $H_s = 0.08$ to 0.60 m, $T_p = 1.0$ to 2.0 s, $n = 0, 2, 10, 20$ and 40 , the results are:

- The acoustic energy of breaking waves varied between 9.0×10^{-7} J and 1.2×10^{-5} J.

- The ratio of the acoustic energy generated by breaking waves to the energy dissipated in breaking waves varied from 1.0×10^{-7} to 4.1×10^{-7} .
- Whitecap coverage varied from 0.005% to 1.26%.
- The best discriminator for breaking waves is the second derivative of the wave height function.

The experimental data provided here may be useful for calibrating the theoretical models of whitecap coverage.

Acknowledgements

I am grateful to Prof. Stanisław Massel and Dr. Jacek Piskozub for their helpful advice and discussion. I am also specially thankful to Marcin Wichorowski M. Eng. for his assistance with the computer programming.

References

- Blanchard D. C., 1971, *Whitecaps at sea*, J. Atmos. Sci., 28, 645 pp.
- Cardone V. J., 1969, *Specification of the wind field distribution in the marine boundary layer for wave forecasting*, Rep. TR 69-1, Geophys. Sci. Lab., New York Univ., New York, 131 pp.
- Carey W. M., Fitzgerald J. W., Monahan E. C., Wang Q., 1993, *Measurements of sound produced by a tapping trough with fresh and salt water*, J. Acoust. Soc. Am., 93 (5), 3178–3192.
- Deane G. B., Stokes M. D., 2002, *Scale dependence of bubble creation mechanisms in breaking waves*, Nature, 418, 839–844.
- Ding L., Farmer D., 1993, *Passive acoustic measurements of scale, probability, and intensity of wave breaking*, Proc. OCEANS '93. 'Engineering in harmony with ocean', 18–21 October 1993, Vol. 2, pp. II/193–II/197.
- Ding L., Farmer D., 1994, *On the dipole source level of breaking waves*, J. Acoust. Soc. Am., 96 (5), 3036–3044.
- Hanson J. L., Phillips O. M., 1999, *Wind sea growth and dissipation in the open ocean*, J. Phys. Oceanogr., 29, 1633–1648.
- Hasselmann K., Barnett T. P., Bouws E., Carlson H., Cartwright D. E., Enke K., Ewing J. A., Gienapp H., Hasselmann D. E., Kruseman P., Meerburg A., Müller P., Olbers D. J., Richter K., Sell W., Walden H., 1973, *Measurements of wind – wave growth and swell decay during the Joint North Sea Wave Project (JONSWAP)*, Dt. Hydrogr. Z., 8 (12), Suppl. A, 1–95.
- Kolaini A. R., 1998, *Sound radiation by various types of laboratory breaking waves in fresh and salt water*, J. Acoust. Soc. Am., 103 (1), 300–308.

- Kolaini A. R., Crum L. A., 1994, *Observations of underwater sound from laboratory breaking waves and implications concerning ambient noise in the ocean*, J. Acoust. Soc. Am., 96 (3), 1755–1765.
- Kraan C., Oost W. A., Janssen P. A. E. M., 1995, *Wave energy dissipation by whitecaps*, J. Atmos. Ocean. Tech., 13 (1), 262–267.
- Longuet-Higgins M. S., 1975, *On the joint distribution of the periods and amplitudes of sea waves*, J. Geophys. Res., 80 (18), 2688–2694.
- Longuet-Higgins M. S., Fox M. J. H., 1977, *Theory of the almost highest wave: the inner solution*, J. Fluid Mech., 80, 721–741.
- Longuet-Higgins M. S., Smith N. D., 1983, *Measurement of breaking waves by a surface meter*, J. Geophys. Res., 88, 9823–9831.
- Massel S. R., 1996a, *Ocean surface waves, their physics and prediction*, World Sci. Publ., Singapore, 431 pp.
- Massel S. R., 1996b, *On the largest wave height in water of constant depth*, Ocean Eng., 23, 553–573.
- Massel S. R., 1998, *The limiting wave height in wind-induced wave trains*, Ocean Eng., 25, 735–752.
- Massel S. R., 2001a, *On the relationship between wave breaking and marine aerosol concentration in deep sea areas*, Arch. Hydro-Eng. Environ. Mech., 48 (2), 31–45.
- Massel S. R., 2001b, *Wavelet analysis for processing of ocean surface wave records*, Ocean Eng., 28, 957–987.
- Massel S. R., Tęgowski J., Chomka M., Wichorowski M., Dąbrowski J., 2001, *Experimental study of the formation of steep waves and breakers*, Oceanologia, 43 (3), 353–363.
- Melville W. K., 1993, *Energy dissipation by breaking waves*, J. Phys. Oceanogr., 24 (10), 2041–2049.
- Monahan E. C., 1969, *Fresh water whitecaps*, J. Atmos. Sci., 26, 1026–1029.
- Monahan E. C., 1971, *Ocean whitecaps*, J. Phys. Oceanogr., 1, 139–144.
- Monahan E. C., 1993, *Occurrence and evolution of acoustically relevant subsurface bubble plumes and their associated, remotely monitorable, surface whitecaps*, [in:] *Natural physical sources of underwater sound*, B. R. Kerman (ed.), Kluwer Acad., Norwell, Mass., 503–517.
- Monahan E. C., O’Muircheartaigh I. G., 1980, *Optimal power-law description of oceanic whitecaps coverage dependence on wind speed*, J. Phys. Oceanogr., 10, 2094–2099.
- Monahan E. C., Zietlow C. R., 1969, *Laboratory comparisons of fresh-water and salt-water whitecap*, J. Geophys. Res., 74, 6961–6966.
- Ochi M. K., Tsai C.-H., 1983, *Prediction of occurrence of breaking waves in deep water*, J. Phys. Oceanogr., 13 (12), 2008–2019.
- Oguz H., 1994, *A theoretical study of low frequency oceanic ambient noise*, J. Acoust. Soc. Am., 95 (4), 1895–1912.

- Orris G. J., Nicholas M., 2000, *Collective oscillations of fresh and salt water bubble plumes*, J. Acoust. Soc. Am., 107 (2), 771–787.
- Ross D. B., Cardone V., 1974, *Observations of oceanic whitecaps and their relation to remote measurements of surface wind speed*, J. Geophys. Res., 79, 444–452.
- Srokosz M. A., 1986, *On the probability of wave breaking in deep water*, J. Phys. Oceanogr., 16 (2), 382–385.
- Stramska M., Petelski T., 2003, *Observations of oceanic whitecaps in the north polar waters of the Atlantic*, J. Geophys. Res., 108 (C3), 1–10.
- Stramski D., Tęgowski J., 2001, *Effects of intermittent entrainment of air bubbles by breaking wind waves on ocean reflectance and underwater light field*, J. Geophys. Res., 106 (C12), 345–360.
- Thorpe S. A., Humphries P. N., 1980, *Bubbles and breaking waves*, Nature, 283, 463–465.
- Toba Y., Chaen M., 1973, *Quantitative expression of the breaking of wind waves on the sea surface*, Rec. Oceanogr. Work. Jpn., 12, 1–11.
- Weissman M. A., Ataktürk S. S., Katsaros K. B., 1984, *Detection of breaking events in a wind-generated wave field*, J. Phys. Oceanogr., 14 (10), 1608–1619.
- Wu J., 1979, *Oceanic whitecaps and sea state*, J. Phys. Oceanogr., 9, 1064–1068.
- Wu J., 1988, *Variation of whitecap coverage with wind stress and water temperature*, J. Phys. Oceanogr., 18, 1448–1453.
- Xu D., Hwang P. A., Wu J., 1986, *Breaking of wind-generated waves*, J. Phys. Oceanogr., 16 (10), 2172–2178.